Applied Mathematics and Computation 217 (2010) 1193–1201

Contents lists available at ScienceDirect

Applied Mathematics and Computation

journal homepage: www.elsevier.com/locate/amc

3D-measurement using a scanning electron microscope

Eduard Reithmeier, Taras Vynnyk *, Thanin Schultheis

Institute of Measurement and Automatic Control, University Hannover, Nienburger Str. 17 30167, Hannover, Germany

ARTICLE INFO

Keywords:
Scanning electron microscope
Photometric method
Shape from shading
Secondary electrons
Backscattered electrons

ABSTRACT

In this paper the improved photometric or the so called "Shape From Shading" method is presented. In comparison to known and established approaches the efficiency of the detector system was considered and the requirements of the cosine Lambert's law for the angle distribution of the emitted electrons are suppressed. The method retrieves more accurate data of sub-micrometer substructures like diffractive optical elements (DOE) due to an increased lateral resolution and works more efficiently than widely used comparable techniques.

1. Introduction

Currently the optical measuring systems are admitted to be a standard measurement instrument for surface measurement. However, these devices have several weak points. The lateral resolution of optical measurement tool is limited by the wavelength of the light and lies in the range between 0.3 and 0.8 μm. Another restriction of the optical microscopes is the limited ability to measure the tilted areas. The maximal measurable inclination angle depends on the numeric aperture (NA) of the objective and is limited to approx. 36° for the non-immersed objectives. Clearly higher lateral resolution (up to 5 nm) can be achieved using scanning electron microscope (SEM). However, it produces only 2D-Images, so the true 3D-Surface can be obtained from multiple SEM – photos using additional reconstruction methods. One of these methods is a photometric or so called "shape from shading" method. Before introducing the algorithm the physical processes occurring during irradiation by primary electrons in SEM will be discussed.

In a SEM (see Fig. 1) electrons are thermionically emitted from the cathode. After acceleration towards the anode they are focused by one or two condenser lenses. The electron beam passes also through pairs of scanning coils, which deflect the beam in the x and y directions, so that it scans in a raster mode over a rectangular area of the sample surface. While interacting with the specimen material, the primary electrons (PE) lose energy by multiple random scatterings. The energy exchange between the primary electrons and the specimen atoms in the area close to the injection hole (1–10 nm) results in creation of the low-energy secondary electrons SE1. The energy of these electrons lies per definition in the range of 0–50 eV. Furthermore, the collisions between electrons lead to the formation of high-energy backscattered electrons (BSE) with energies >50 eV. On the way out of the material the BSE produce another low energy secondary electrons SE2, see Fig. 3. The source area for both SE2 and BSE is much larger than for SE1 and depends on the energy of the primary electrons and the irradiated material. So, for the PE-energy of 10–20 keV the diameter of the excited spot of the surface lies in the range of 0.1–1 μm and it decreases to 5–30 nm at lower energies of the primary electrons. The BSE can also produce SE3 while contacting the chamber walls. However, these electrons can be eliminated and therefore will be not discussed in this paper anymore.

* Corresponding author.
E-mail address: sekretariat@imr.uni-hannover.de (T. Vynnyk).

0096-3003/$ - see front matter © 2010 Elsevier Inc. All rights reserved.
doi:10.1016/j.amc.2010.01.107

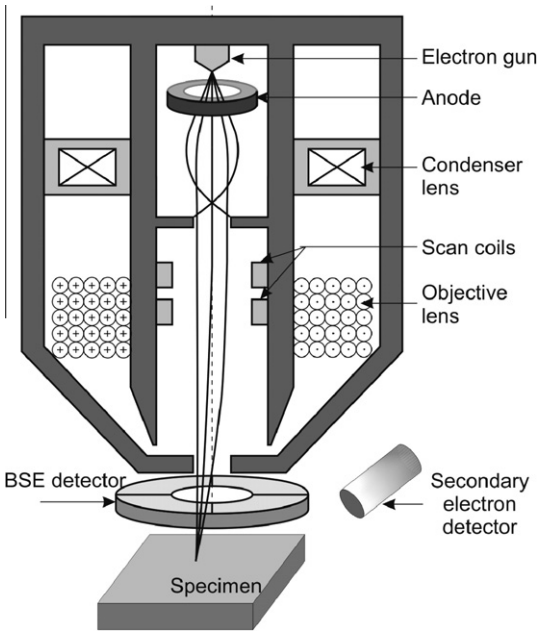

Fig. 1. Schematic diagram of SEM.

2. Idea of the photometric method

The basics of the photometric method were developed in the 90's [1]. The method assumes that the emission yield $\sigma(\phi)$ depends on the local inclination angle of the specimen ϕ as: $\sigma(\phi) = \sigma_0/\cos(\phi)$. Besides, the angle distribution of the emitted electrons follows the Lambert cosine law: $f(\psi) = \cos(\psi)$. If a symmetrical 2-detector system is used for registration of the emitted electrons [2,5], see Fig. 2, then the detector signals I_1 and I_2 can be presented as $I_{1,2} = \frac{1}{2} \cdot \sigma(\varphi) \cdot (1 \mp \sin\varphi)$ and therefore the difference is:

$$I_2 - I_1 = \sigma_0 \cdot \tan\varphi = \sigma_0 \cdot \frac{dz(x,y)}{dx}. \tag{1}$$

Finally, the surface profiles can be reconstructed via numerical integration of the partial derivatives.

Despite the simple reconstruction algorithm, the photometric method was not established as standard measuring method due to the following reasons:

1. The material dependent emission coefficient σ_0 in Eq. (1) is unknown.
2. The photometric method assumes that the emission yield behaves as $\cos^{-1}$ of the local inclination angle of the measured specimen. This assumption is correct only for primary electrons with the energy > 10 keV, see Fig. 3. However, the use such primary electrons increases both the BSE-fraction and the emission volume (electron range), which leads to loss of the lateral resolution. Besides, the angular distribution of BSE strongly depends on the incident angle of the primary electron beam.

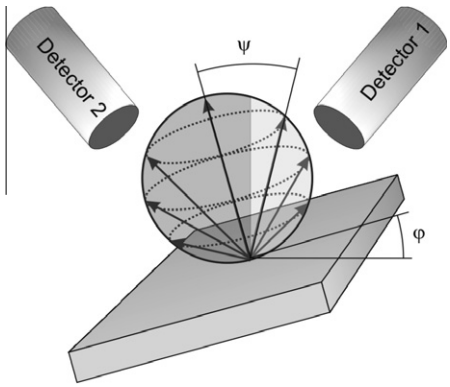

Fig. 2. 2-detector system.

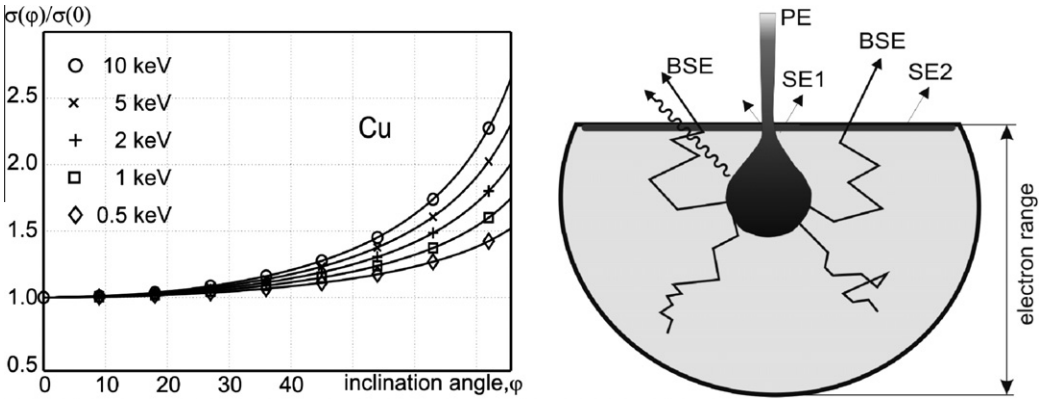

Fig. 3. Dependence of the emission yield on the inclination angle (left) and occurence of the secondary electrons (right).

3. The angular distribution of the secondary emission electrons (SE) is assumed to have a cosine form. This assumption is a very rough approximation of the real one. The alternative approach refers to quantum mechanics and gives more realistic description of its behaviour [3].
4. The efficiency factor of the detector system is supposed to be one. In reality the efficiency is always smaller due to the influence of the specimen chamber and of the electron gun. According to the recent publications the efficiency of one ET Detector lies approximately about 30–40% [4].

3. Improvements

For successful implementation of the photometric method the conventional scanning electron microscope (SEM) is to be equipped with 4 Everhardt Thornley (ET) detectors. Two of them should be oppositely positioned along the *x*-axis and two - along the *y*-axis. Alternatively, a 2-detector system and a rotation unit around the *z*-axis can be used. This rotation unit gives an opportunity, to position the ET-detectors firstly along the *x*- and finally along the *y*-axis and thus to determine the partial derivatives of the measured surface.

The reconstruction formulas are based on the following assumptions:

1. The angle distribution takes the following form:

$$f(\psi) = \frac{1}{\pi} \cdot (k_1 \cdot \cos\psi - k_2 \cdot \cos^2\psi). \tag{2}$$

Here ψ describes the angle between the direction of the emitted electron and the normal to the local tangent plane to the surface in the measured position. The coefficients k_1 and k_2 are determined via parameter optimization on experimental data. Such an approach allows being more flexible while describing the angular distribution comparing to the Lambert's cosine law.

2. The emitted electrons are registered either by one of the 2 detectors or captured by the surface or the electron gun [3]. Based on the FEM simulation results the emission directions were split in 3 zones. The Zone 1 stands for the electrons being registered by the detectors. Zone 2 represents electrons, which are captured theoretically neither by the detectors nor by the electron gun. Nevertheless they are considered as being registered to 50% by detector 1 and 50% by detector 2. Zone 3 describes electrons, which are partly absorbed by the electron gun. To describe this zone splitting two angle parameters are introduced. The first parameter corresponds to half of the opening angle θ of Zone 3, which describes its partial absorption. The second parameter describes the maximum azimuthal angle β, at which the emission electrons are registered by the respective detector, see Fig. 4. Both of these parameters depend on the distance between the specimen and the electron gun. Furthermore the angle θ can be influenced by the applied voltage to the bottom facet of the electron gun. So, a voltage of about 10V reduces θ significantly and thus increases the efficiency of the detector system.

3.1. Zone 1

In order to eliminate the influence of the electron gun the θ angle will be temporally set to 0°. Since this marginal ($\theta = 0°$) case is used for further considerations, Zone 1 here is defined as $Zone_{1\_0°}$. The electron flow via elementary surface element $dG = r^2 \cdot d\Omega$, see Fig. 5, is:

$$d\Phi = \sigma(x,y) \cdot f(\gamma,\alpha) \cdot r^{-2} \cdot dG = \sigma(x,y) \cdot (k_1 \cdot f_{Lam}(\gamma,\alpha) - k_2 \cdot f_{Lam}^2(\gamma,\alpha)) \cdot d\Omega, \tag{3}$$

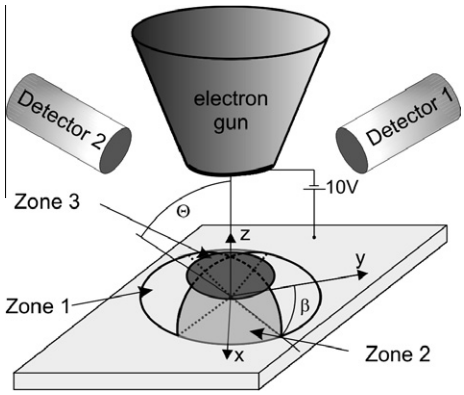

Fig. 4. Zone splitting of the emitted electrons.

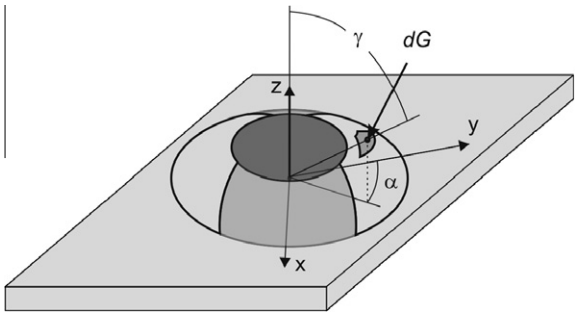

Fig. 5. Electron flow over the elementary surface.

where $d\Omega$ is a differential solid angle, $r = 1$ – the radius of the unit sphere and $f(\gamma,\alpha)$ – the angular distribution of the emitted electrons in the global spherical coordinate system. This distribution depends on zenith angle γ and azimuth angle α as shown in Fig. 5. As already mentioned in Eq. (2), the angular distribution is a superposition of the Lambert's (cosine) $f_{Lam}(\gamma,\alpha)$ and square Lambert's $f^2_{Lam}(\gamma,\alpha)$ functions. For arbitrary direction $\vec{r}(\gamma,\alpha) = [\sin\gamma\cdot\sin\alpha, \sin\gamma\cdot\cos\alpha, \cos\gamma]$ the Lambert's distribution takes the following form:

$$f_{Lam}(\gamma,\alpha) = \cos(\vec{r},\vec{n}) = \frac{-1}{\pi}\cdot\sqrt{1+\frac{\partial z^2}{\partial x}+\frac{\partial z^2}{\partial y}}^{-1}\cdot\left(\frac{\partial z}{\partial x}\cdot\sin\gamma\cdot\sin\alpha+\frac{\partial z}{\partial y}\cdot\sin\gamma\cdot\cos\alpha-\cos\gamma\right). \tag{4}$$

Here $\vec{n}$ is the normal to the tangent plane of the surface at the irradiation point: $\vec{n} = \left[-\frac{\partial z}{\partial x}, -\frac{\partial z}{\partial y}, 1\right]^T$

The signals on the detectors 1 and 2 are proportional to the electron flow Φ and can be calculated as surface integrals:

$$\frac{I_{1y,2y}}{\sigma(x,y)} = \int_{\Omega_{1,2}} f(\gamma,\alpha)\cdot d\Omega = k_1\cdot\underbrace{\int_a^b d\alpha\int_0^{\theta(\alpha)} f_{Lam}(\gamma,\alpha)\cdot\sin\gamma\cdot d\gamma}_{Int_{11}(a,b)} - k_2\cdot\underbrace{\int_a^b d\alpha\int_0^{\theta(\alpha)} f^2_{Lam}(\gamma,\alpha)\cdot\sin\gamma\cdot d\gamma}_{Int_{12}(a,b)}, \tag{5}$$

with $\sigma(x,y)$ as the total emission yield and $\Omega_{1,2}$ as integration domains for the detectors 1 and 2. In the Cartesian coordinate system these signals can be represented as double integrals over the domain presented via azimuth range $[a,b]=[-\beta,\beta]$ and $[a,b]=[\pi-\beta,\pi+\beta]$ for detectors 1 and 2 respectively and zenith range $[0\cdot\cdot\theta(\alpha)]$. The upper integration limit $\theta(\alpha)$ is defined as the intersection of the tangent plane and the azimuth integration plane $x\cdot\cos\alpha - y\cdot\sin\alpha = 0$, see also Fig. 6:

$$\theta(\alpha) = \arccos\left(M\cdot\sqrt{1+M^2}^{-1}\right),\quad M = \sin\alpha\cdot\frac{\partial z}{\partial x}+\cos\alpha\cdot\frac{\partial z}{\partial y}. \tag{6}$$

After substitution using Eqs. (4) and (6) and simplification the integral $Int_{11}(a,b)$ Eq. (5) takes the following form:

$$Int_{11}(a,b) = \frac{1}{2\pi}\cdot\sqrt{1+\frac{\partial z^2}{\partial x}+\frac{\partial z^2}{\partial y}}^{-1}\cdot\int_a^b\left(1-\left(\sin\alpha\cdot\frac{\partial z}{\partial x}+\cos\alpha\cdot\frac{\partial z}{\partial y}\right)\cdot\theta(\alpha)\right)\cdot d\alpha. \tag{7}$$

Unfortunately this integral cannot be solved via elementary functions. However, for the surface reconstruction using only $Zone_{1\_0^\circ}$ not the signals but their difference is significant:

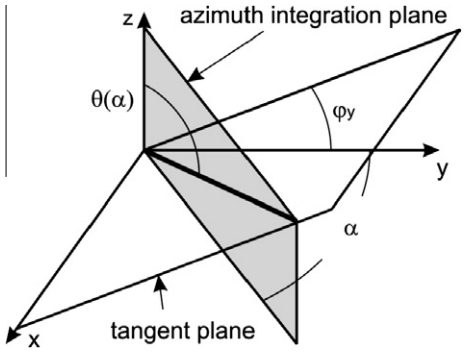

Fig. 6. Evaluation of the upper integration limit.

$$\frac{I_{2y}-I_{1y}}{\sigma(x,y)} = k_1 \cdot \underbrace{(Int_{11}(\pi-\beta,\pi+\beta)-Int_{11}(-\beta,\beta))}_{\Delta Int_{11}} - k_2 \cdot \underbrace{(Int_{12}(\pi-\beta,\pi+\beta)-Int_{12}(-\beta,\beta))}_{\Delta Int_{12}}. \tag{8}$$

The use of relations $\cos(\alpha+\pi) = -\cos\alpha, \sin(\alpha+\pi) = -\sin\alpha, \theta(\alpha+\pi) = \pi-\theta\ (\alpha)$ leads to:

$$\Delta Int_{11} = \sin\beta \cdot \sin\varphi_y, \tag{9}$$

whereas the inclination angles φ_x, φ_y are defined as:

$$\sin\varphi_y = \frac{\partial z}{\partial y}\cdot\sqrt{1+\frac{\partial z^2}{\partial x}+\frac{\partial z^2}{\partial y}}^{-1}, \quad \sin\varphi_x = \frac{\partial z}{\partial x}\cdot\sqrt{1+\frac{\partial z^2}{\partial x}+\frac{\partial z^2}{\partial y}}^{-1}. \tag{10}$$

The second integral Int_{12} is treated in the similar way:

$$\begin{aligned} Int_{12}(a,b) &= \frac{1}{3\pi}\left(1+\frac{\partial z^2}{\partial x}+\frac{\partial z^2}{\partial y}\right)^{-1}\cdot\int_a^b (1+(2-3\cdot\cos\theta+\cos^3\theta)\cdot M^2 - 2\cdot\sin^3\theta\cdot M-\cos^3\theta)\cdot d\alpha, \\ M &= \sin\alpha\cdot\frac{\partial z}{\partial x}+\cos\alpha\cdot\frac{\partial z}{\partial y}. \end{aligned} \tag{11}$$

After simplification of the Int_{12} the integral difference ΔInt_{12} from Eq. (8) can be solved using elementary functions:

$$\Delta Int_{12} = \frac{2}{3\pi}\cdot\left(X\cdot\sqrt{1-X^2}+\arcsin X\right)\Big|_{-\beta}^{\beta}, \quad X(\alpha) = \sin\alpha\cdot\sin\varphi_y - \cos\alpha\cdot\sin\varphi_x. \tag{12}$$

Despite ΔInt_{12} can be solved analytically, due to its complexity it can be barely used for further considerations and therefore it will be approximated using elementary functions. One of the possible approximations is the decomposition of the primitive function ΔInt_{12} using Taylor series [7], see Eq. (12):

$$\frac{1}{2}\cdot\left(X\cdot\sqrt{1-X^2}+\arcsin X\right) = X-\frac{1}{6}X^3-\frac{1}{40}X^5-\frac{1}{112}X^7+O(X^9). \tag{13}$$

At small slope angles $X \ll 1$, hence for the characterization of the behaviour of the primitive function, the linear and cubic member of the Taylor Eq. (13) series are sufficient:

$$\Delta Int_{12} = \frac{8}{3\pi}\cdot\sin\beta\cdot\sin\varphi_y\cdot(1-\kappa\cdot 3\cos^2\beta+\kappa\cdot(3\cos^2\beta-\sin^2\beta)\cdot\sin^2\varphi_y+\kappa\cdot 3\cos^2\beta\cdot\cos^2\lambda), \tag{14}$$

with $\kappa \approx 1/5.8$ and λ as the angle between the z axis and the normal to the tangent plane:

$$\cos\lambda = \sqrt{1+\frac{\partial z^2}{\partial x}+\frac{\partial z^2}{\partial y}}^{-1} = \sqrt{1-\sin^2\varphi_x-\sin^2\varphi_y}. \tag{15}$$

Finally, after evaluation of the integrals ΔInt_{11} and ΔInt_{12} the difference of the detector signals for $Zone_{1\_0^\circ}$ can be determined as:

$$I_{2y}-I_{1y} = \sigma(x,y)\cdot\sin\beta\cdot\sin\varphi_y\cdot\left(c_1+c_2\cdot\sin^2\varphi_y+c_3\cdot\cos^2\lambda\right), \tag{16}$$

whereas the coefficients $c_1 \ldots c_3$ are the functions of the angle parameters β and θ. These functions are determined in Eqs. (8), (9) and (14). The sum of the detector signals depends only from Zone 3 and in case of $\theta = 0^\circ$ is equal to the total emission yield at the irradiation point:

$$I_{2y} + I_{1y} = \sigma(x,y). \tag{17}$$

3.2. Zone 3

Next the influence of the Zone 3 will be examined. Similarly to the calculation procedures for Zone 1, Zone 3 is also divided into elementary surfaces and the entire electron flow is computed as integral sum, see also Eq. (3):

$$\frac{I_{Zone3}}{\sigma(x,y)} = k_1 \cdot \underbrace{\int_{-\pi}^{\pi} d\alpha \int_0^{\theta} f_{Lam}(\gamma,\alpha)\cdot\sin\gamma\cdot d\gamma}_{Int_{31}(-\pi,\pi)} - k_2 \cdot \underbrace{\int_{-\pi}^{\pi} d\alpha \int_0^{\theta} f_{Lam}^2(\gamma,\alpha)\cdot\sin\gamma\cdot d\gamma}_{Int_{32}(-\pi,\pi)}, \tag{18}$$

where $\theta = const$ is the maximal angle, with which the emission electrons are absorbed by electron gun. Both components $Int_{31}(a,b)$ and $Int_{32}(a,b)$ of the electron flow over Zone 3 in Eq. (18) are expressed as functions of the integration limits:

$$Int_{31}(a,b) = \frac{1}{2\pi}\cdot\sqrt{1+\frac{\partial z^2}{\partial x}+\frac{\partial z^2}{\partial y}}^{-1}\cdot\int_a^b (M\cdot(\cos\theta\cdot\sin\theta-\theta)+\sin^2\theta)\cdot d\alpha,\ M = \sin\alpha\cdot\frac{\partial z}{\partial x}+\cos\alpha\cdot\frac{\partial z}{\partial y}, \tag{19}$$

$$Int_{32}(a,b) = \frac{1}{3\pi}\cdot\left(1+\frac{\partial z^2}{\partial x}+\frac{\partial z^2}{\partial y}\right)^{-1}\cdot\int_a^b (1+(2-3\cos\theta+\cos^3\theta)\cdot M^2 - 2\sin^3\theta\cdot M - \cos^3\theta)\cdot d\alpha. \tag{20}$$

Unlike to Zones 1 and 2 the electron flow over Zone 3 is considered to be partly absorbed by the electron gun, which leads to a decrease of the sum of detector signals:

$$\frac{I_{1y}+I_{2y}}{\sigma(x,y)} = 1-\tau\frac{I_{Zone3}}{\sigma(x,y)} = 1-\tau\cdot k_1\cdot Int_{31}(-\pi,\pi)+\tau\cdot k_2\cdot Int_{32}(-\pi,\pi) = a_0 - a_1\cdot\cos\lambda + a_2\cdot\cos^2\lambda. \tag{21}$$

Here τ is the absorption coefficient of the electron gun and $a_0 = 1+\tau\cdot k_2\cdot\frac{1}{3}\cdot(2-3\cdot\cos\theta+\cos^3\theta)$, $a_1 = \tau\cdot k_1\cdot\sin^2\theta$, $a_2 = \tau\cdot k_2\cdot(\cos\theta-\cos^3\theta)$ are system specific constants.

Since the non-absorbed fraction of the emission electrons over Zone 3 is assumed to be split in half between the detectors 1 and 2, it does not affect the difference of the detector signals. Therefore the entire difference of detector signals can be expressed as the signal difference over $Zone_{1\_0^\circ}$ subtracting the absorbed electrons over the intersection of Zone 3 and $Zone_{1\_0^\circ}$:

$$I_{2y} - I_{1y} = I_{2y}(Zone_{1\_0^\circ}) - I_{1y}(Zone_{1\_0^\circ}) + I_{1y}(Zone_3\cap Zone_{1\_0^\circ}) - I_{2y}(Zone_3\cap Zone_{1\_0^\circ}) \tag{22}$$

For the difference $\Delta I_{Zone_3} = I_{1y}(Zone_3\cap Zone_{1\_0^\circ}) - I_{2y}(Zone_3\cap Zone_{1\_0^\circ})$ following equation is valid:

$$\frac{\Delta I_{Zone_3}}{\sigma(x,y)} = k_1\cdot\underbrace{(Int_{31}(-\beta,\beta)-Int_{31}(\pi-\beta,\pi+\beta))}_{\Delta Int_{31}} - k_2\cdot\underbrace{(Int_{32}(-\beta,\beta)-Int_{32}(\pi-\beta,\pi+\beta))}_{\Delta Int_{32}}. \tag{23}$$

The integration of summands leads to:

$$\Delta Int_{31} = -\frac{1}{\pi}\cdot(2\theta-\sin(2\theta))\cdot\sin\beta\cdot\sin\varphi_y, \tag{24}$$

$$\Delta Int_{32} = -\frac{8}{3\pi}\cdot\sin^3\theta\cdot\sin\beta\cdot\sin\varphi_y\cdot\cos\lambda. \tag{25}$$

Thus the signal relation with consideration of the efficiency of the detector system can be represented as follows:

$$k_y(x,y) = \frac{I_{2y}-I_{1y}}{I_{2y}+I_{1y}} = \sin\varphi_y\cdot\sin\beta\cdot\frac{b_1+b_2\cdot\sin^2\varphi_y+b_3\cdot\cos^2\lambda+b_4\cdot\cos\lambda}{a_0-a_1\cdot\cos\lambda+a_2\cdot\cos^2\lambda}. \tag{26}$$

The coefficients from the Eq. (26) are summarized in Table 1.

The presented signal relation refers to detectors, aligned along the y axis. The computation for the detectors along the x axis is similar, hence:

$$k_x(x,y) = \frac{I_{2x}-I_{1x}}{I_{2x}+I_{1x}} = \sin\varphi_x\cdot\sin\beta\cdot\frac{b_1+b_2\cdot\sin^2\varphi_x+b_3\cdot\cos^2\lambda+b_4\cdot\cos\lambda}{a_0-a_1\cdot\cos\lambda+a_2\cdot\cos^2\lambda}. \tag{27}$$

Table 1
Coefficients of the signal relation.

$b_1 = k_1\cdot(1+\frac{1}{\pi}\cdot(\sin(2\theta)-2\theta))-\frac{8}{3\pi}\cdot k_2\cdot(1-3\kappa\cdot\cos^2\beta)$	$b_2 = k_2\cdot\frac{8\kappa}{3\pi}\cdot(\sin^2\beta-3\cdot\cos^2\beta)$
$b_3 = -k_2\cdot\frac{8\kappa}{\pi}\cdot\cos^2\beta$	$b_4 = k_2\cdot\frac{8}{3\pi}\sin^3\theta$
$a_0 = 1+k_2\cdot\frac{1}{3\tau}\cdot(2-3\cdot\cos\theta+\cos^3\theta)$	$a_1 = \tau\cdot k_1\cdot\sin^2\theta$
$a_2 = \tau\cdot k_2\cdot(\cos\theta-\cos^3\theta)$	$\kappa\approx\frac{1}{5.8}$

4. Influence of the specimen

To complete modelling of the signal, the influence of the surface must be considered, because the electrons with a small emission angle are partly absorbed by the surface. For the quantitative evaluation of the unregistered fraction of the emitted electrons the maximal directly registered angle $\phi_{\max}$ should be determined. This parameter defines the maximal angle, at which the electrons are still not absorbed through the surface of the specimen. The evaluation of this angle has to be made for each measuring point (x,y), and for each azimuth emission angle α, see Fig. 7. Respecting zone splitting, the unregistered emission fraction can be calculated as:

$$\xi(x,y,\beta_1,\beta_2) = \frac{k_1}{2\pi}\int_{\beta_1}^{\beta_2} \cos^2\varphi_{\max}(\alpha)\cdot d\alpha - \frac{k_2}{2\pi}\int_{\beta_1}^{\beta_2} \cos^3\varphi_{\max}(\alpha)\cdot d\alpha. \tag{28}$$

Hereby β_1 and β_2 describe the lateral angle-borders of Zone 1.

Finally, the signal relation for detectors, aligned along the y axis, which is the main equation of the presented mathematical model, takes the following form:

$$ky = \frac{I_{2y}(x,y) - I_{1y}(x,y)}{I_{2y}(x,y) + I_{1y}(x,y)} = \frac{\sin\psi_y \cdot Nom \cdot \sin\beta - \tau\cdot\left[\xi\left(-\beta+\frac{\pi}{2},\beta+\frac{\pi}{2}\right) - \xi\left(-\beta-\frac{\pi}{2},\beta-\frac{\pi}{2}\right)\right]}{Den - \tau_{sp}\cdot\xi(-\pi,\pi)}. \tag{29}$$

Here: I_{1y}, I_{2y} – measured detector signals, τ_{sp}, τ – absorption coefficients of the specimen and of the electron gun.

Further components of the Eq. (29) describe the dependence of the signal relation on the local inclination angle: $Nom = b_1 + b_2\cdot\sin^2\psi_y + b_3\cdot\cos^2\lambda + b_4\cdot\cos\lambda$,$Den = a_0\text{-}a_1 + a_2\cdot\cos^2\lambda$ where the coefficients $a_0\ldots a_2$ and $b_1\ldots b_4$ are determined in Table 1 as functions of the previously mentioned system parameters θ and β. These system parameters depend on the hardware constellation of SEM, like working distance, initial electron energy etc., and can be evaluated using different optimization techniques [6,7]. One of these techniques is the method of the maximum likelihood estimation on the calibration steel ball with the diameter of 1 mm. Because the height values are measured indirectly over the detector signal relations, the target function refers to the measured and modelled signal relations, see Eq. (29):

$$ZF = \sum_{i,j=1}^{N,M}\left[k_{xij} - k_x(x_i,y_j;a_0..a_2,b_1..b_4)\right]^2 + \sum_{i,j=1}^{N,M}\left[k_{yij} - k_y(x_i,y_j;a_0..a_2,b_1..b_4)\right]^2 \to \underbrace{\min}_{a_0..a_2,b_1..b_4}, \tag{30}$$

with k_x, k_y as model based and k_{xij}, k_{yij} as experimentally obtained signal relations.

The unknown coefficients $a_0\ldots a_2$ and $b_1\ldots b_4$ are based on:

- k_1, k_2 – weight coefficients of the angular distribution in Eq. (2).
- τ, τ_{sp} – absorption coefficients.
- θ, β – angle parameters for zone splitting.

The signal relations has to be determined along the y- and the x-axis. So, for each point (x,y) two equations exist, connecting the detector signals, surface function $z(x,y)$ and the partial derivatives z'_x and z'_y. Because $z(x,y)$ is unknown, the reconstruction algorithm is an iterative procedure:

1. At the 0-Iteration the surface is considered to be constant: $z(x,y) = 0$ and the partial derivatives are computed using Eq. (29).

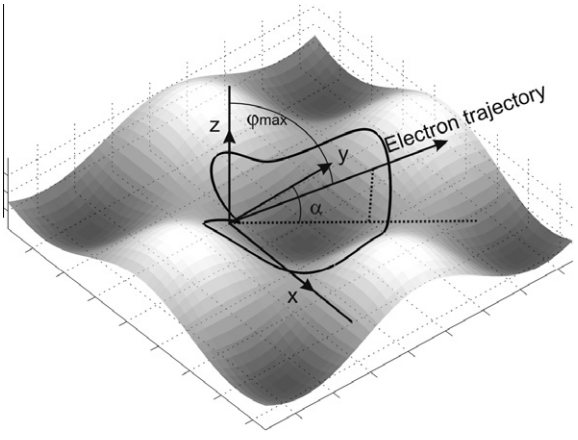

Fig. 7. Unregistered emission fraction.

2. Numeric integration of the partial derivations, which results in the new approximation of the real surface.
3. Based on the in step 2 reconstructed surface, the unregistered fractions of the emitted electrons are re-computed using Eq. (28). These fractions act as basement for the re-evaluation of the partial derivatives with Eq. (29).
4. If the difference between the partial derivatives z'_x and z'_y, computed in two sequential iterations is smaller than the given threshold, the algorithm will be terminated; otherwise the iteration will be repeated. Usually the computed surface converges very fast against the real one.

5. Experiments

To examine the accuracy of measurement a steel ball of 1 mm diameter was used. As Fig. 8 shows, for small slope angles the 3D reconstruction fits a nearly perfect spherical shape. After reaching a slope angle of approximately 45°, the deviation in the height increases strongly.

This circumstance can be explained by the non unique correspondence between the signal relation $k_x = (I_{2x} - I_{1x}) \cdot (I_{2x} + I_{1x})^{-1}$ and the local slope angle, as it is shown in Fig. 9. Here the ball is positioned in the centre of the image, so the inclination decreases monotonically along the marked lines. In contrast to the inclination, the signal relation k_x can be distinguished as a monotonically decreasing function only for small slope angles. After reaching the turning point at around 45° the signal relation k_x changes its orientation. The angle of this turning point depends on the SEM and can be increased significantly by taking proper precautions like shielding the electron gun [2]. While reconstructing, the slope is derived out of the signal relation where an ambiguity of the determination of the surface gradient occurs and smallest possible slope will be chosen.

For slope angles between 0° and 45° the deviation is less than 5 µm. Though the deviation of the measuring results is relatively large, it is crucial that the reconstruction algorithm is only connected to the slope and therefore linearly dependent on the dimension of the sample. If, for example, a steel ball of 10 µm diameter is measured an accuracy of approximately 50 nm can be expected.

The advantages of the SEM over optical measuring methods will be highlighted with a holographic diffractive grating of 830 nm. Because of the physical resolution restriction of about 200 nm, the optical measuring devices are at their limit although the grating period length is relatively large. While the sine wave is identifiable with 100× magnification, it can't be measured with 50× magnification due to poor lateral resolution of 300 nm per pixel, as it is shown in Fig. 10.

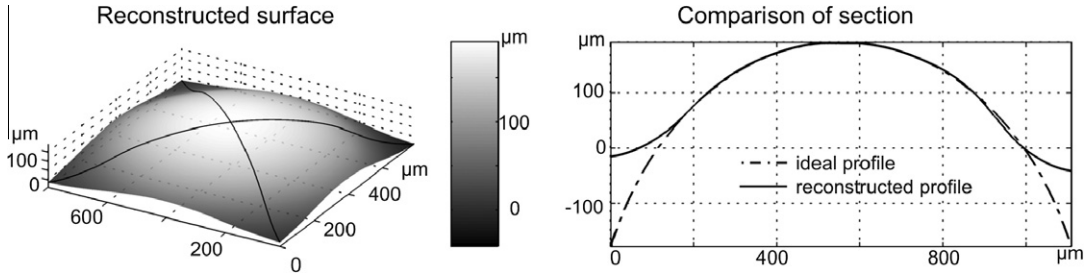

Fig. 8. 3D reconstruction of steel ball: total reconstruction result (left), marked diagonal profiles and corresponding profile (right).

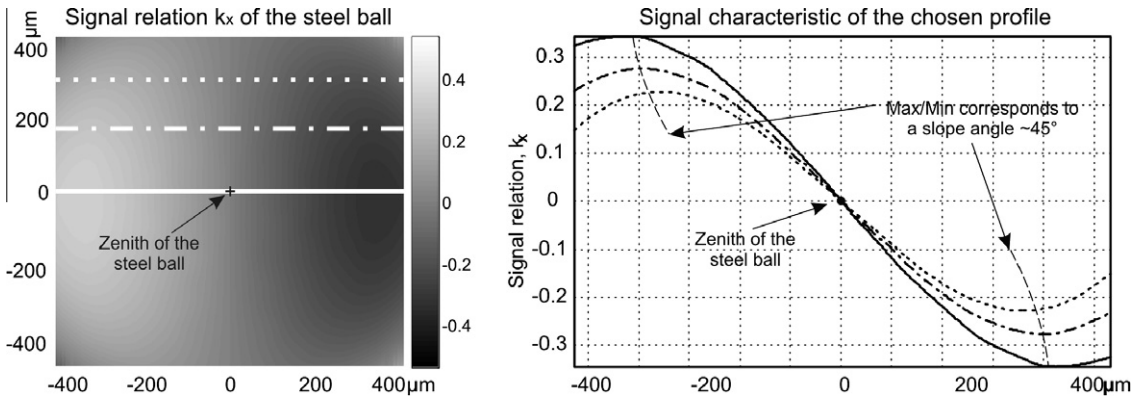

Fig. 9. Calculated signal relation k_x of the steel ball.

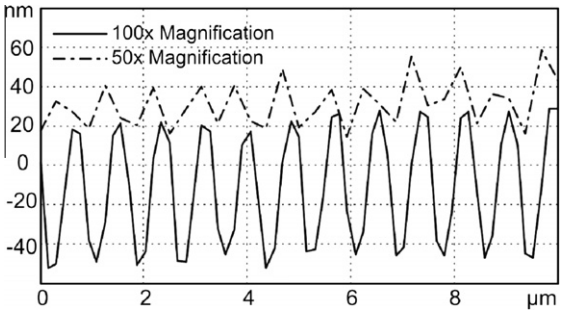

Fig. 10. Measurement of a holographic diffractive grating with a confocal microscope.

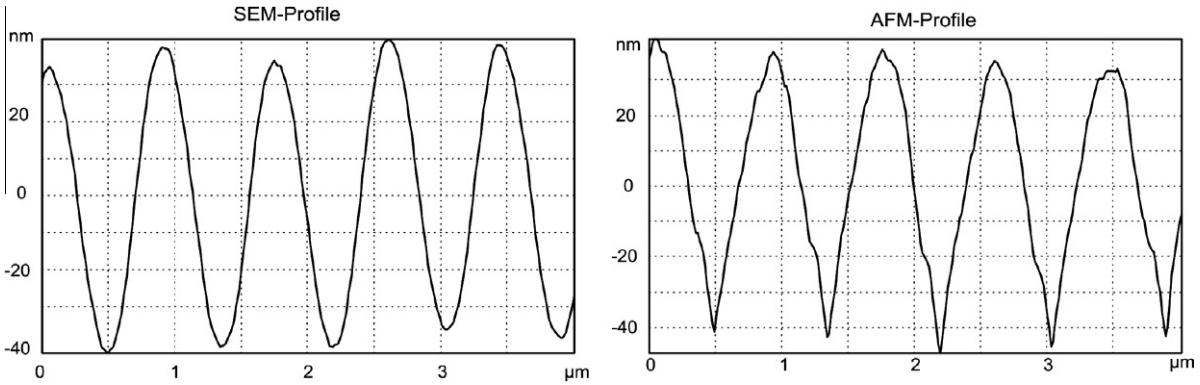

Fig. 11. Comparison between SEM and AFM measurement results.

Since tactile measuring methods might damage the surface they also cannot be used for collecting topography data. Though the atomic force microscope (AFM) in non-contact mode is able to fulfil the measuring task, the time effort is so tremendous that measuring objects with higher complexity like holograms is not feasible in a reasonable amount of time. Fig. 11 shows the SEM and AFM measurement results. Due to the homogeneous character of the grating surface, an exact localization of the measuring position and therefore the comparison between the two different methods is barely possible. Nonetheless a structural height of 60–80 nm is noticeable in both, the SEM and the AFM, measurements. While it took the SEM about 10–20 min, the AFM required more than 6 h. In addition the SEM can be operated interactively, while it is nearly impossible to do repetitive measurements with the AFM after changing the sample's position.

6. Conclusions

In this paper a mathematical model of the improved photometric method was introduced, which can be summarized with Eq. (29). The presented results prove that the modified SEM method is suitable to use for investigations of flat structures to obtain high lateral resolution data (30 nm). This method gives the possibility to measure DOEs with a reasonable effort of time, where optical and tactile measuring devices fail. For the measurement of structures with a slope angle above 45° an improvement of the setup is needed. This can be fulfilled by reducing the influence of the electron gun.

Acknowledgement

This research was partially funded by the German Research Foundation (DFG)under grants RE1488/11-3 and FA887/1-1.

References

[1] L. Reimer, Image Formation in Low-Voltage Scanning Electron Microscopy, SPIE Press Book, 1993.
[2] M. Kässens, L. Reimer, Contrast effects using a 2-detector system in low voltage scanning electron microscopy, Journal of Microscopy 181 (1996) 277–285.
[3] J. Cazaux, Recent developments and new strategies in scanning electron microscopy, Journal of Microscopy 217 (2005) 16–35.
[4] I. Müllerova, I. Konvalina, Collection of secondary electrons in scanning electron microscopes, Journal of Microscopy (2009).
[5] E. Reithmeier, T. Vynnyk, An Improved Method to Detect Riblets on Surfaces in Nanometer Scaling Using SEM; From Nano to Space, Applied Mathematics Inspired by Roland Bulirsch (2008).
[6] G. Leitmann, Calculus of Variations and Optimal Control, Plenum Press, New York, 1981. ISBN 0-306-40707-8.
[7] I.N. Bronstein, K.A. Semendyayev, Handbook of Mathematics, Springer; fifth ed., 2007. ISBN 978-3540721215.